Modeling and Experimental Analysis of the Transient Overvoltages on Machine Windings Fed by PWM Inverters

Mohammed Khalil Hussain, Pablo Gomez

***Abstract*-- PWM inverters are widely used in many power applications, including the speed and torque control of motors. However, PWM-type excitation produces electrical stresses in the machine winding due to fast voltage rise times caused by high frequency switching. This phenomenon is magnified by the presence of the feeder cable. In this paper, a non-uniform transmission line model of the machine winding is used to predict the transient propagation of fast pulses along the overhang and slot regions of the coil under fast PWM-excitation. The machine parameters are computed using the finite element method. The cable is included by means of a distributed parameter model whose parameters are obtained from measurements. An experimental coil setup is developed to assess the simulation results. The effect of different rise times from the PWM and different cable lengths in the transient overvoltage along the machine winding are analyzed by means of simulations and measurements.**

***Keywords*: Machine winding, transient overvoltage, non-uniform transmission line, PWM.**

I. Introduction

TRANSIENT overvoltages due to lighting and switching operations have to be considered in the design of machine windings. These overvoltages may cause dielectric stresses leading to insulation failure [1]. Since the 1980s, several computer-based MTL (multiconductor transmission line) modeling approaches have been proposed to predict the magnitude and distribution of transient overvoltage in machine windings under fast-front pulses [2]-[4]. The computation of parameters for this type of models is obtained using analytical or numerical approaches and considering the relationship between inductance, capacitance and wave velocity in homogeneous media for the overhang and slot regions [1], [5]-[9]. The inclusion of frequency dependence in the machine winding parameters has also been reported [2], [10].

In the last decades, induction machines fed by PWM (pulse width modulation) have been widely used in many industrial applications for speed and torque control [9], [16]. PWM-ASDs (adjustable speed drives) have a lot of advantages in terms of performance, size and efficiency. However, they also produce an increase in transient overvoltages as well as insulation stress [11]-[14]. In addition, in many industrial applications it is common to connect the motor and PWM inverter by means of a long cable [12], [15]. These cables further amplify the undesired overvoltages in the motor windings. The magnitude of these overvoltages depends on the pulse rise time and on the characteristic impedance and length of the cable [17]-[18]. Example of cable models used for the simulation of the transient response of an inverter-cable-machine winding setup are described in [17]-[19].

In this paper, the computer model of a machine winding is implemented by means of a non-uniform MTL approach in order to consider the pulse propagation related to an inverter excitation in the two regions occupied by the coil: slot and overhang. The model used is based on the cascaded connection of chain matrices corresponding to each region of the coil. The parameters of the machine winding are calculated from FEM simulations considering nonhomogeneous media composed of different insulation layers. A frequency domain distributed parameter model of the cable is included in the simulations in order to consider its effect in the transient response of the winding when fed by a PWM-type excitation.

II. Modeling of Machine Winding

A schematic representation of the system under study is shown in Fig. 1. A PWM-type excitation is connected through a single-phase cable to the machine winding coil from a medium-voltage form-wound machine. The typical coil of a machines winding has two regions: slot and overhang, as shown in Fig. 1. A constant lumped resistance R_{Term} is used to represent the rest of winding after the first coil.

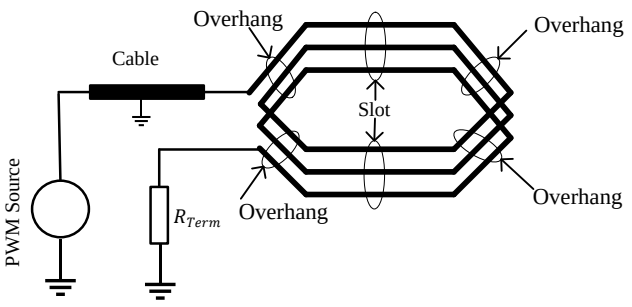

Fig. 1. Schematic model of a form wound stator coil (3 turns are considered for the purpose of illustration) with connecting cable.

M. K. Hussain and P. Gomez are with the Department of Electrical and Computer Engineering of Western Michigan University, Kalamazoo, MI 49008 USA (e-mail: mohammedkhalil.hussain@wmich.edu and pablo.gomez@wmich.edu).

Paper submitted to the International Conference on Power Systems Transients (IPST2017) in Seoul, Republic of Korea June 26-29, 2017

A. Non-uniform line model

The voltage and current waves' propagation along a non-uniform multiconductor transmission line are described by the following equation [20]-[22]:

$$\frac{d}{dt}\begin{bmatrix}\mathbf{V}(x,s)\\ \mathbf{I}(x,s)\end{bmatrix}=\begin{bmatrix}\mathbf{0} & -\mathbf{Z}(x,s)\\ -\mathbf{Y}(x,s) & \mathbf{0}\end{bmatrix}\begin{bmatrix}\mathbf{V}(x,s)\\ \mathbf{I}(x,s)\end{bmatrix} \quad (1)$$

where $\mathbf{V}(x,s)$ and $\mathbf{I}(x,s)$ are the voltage and current vectors in the Laplace domain at any point x, $\mathbf{Z}(x,s)$ and $\mathbf{Y}(x,s)$ are the longitudinal impedance and transversal admittance matrices per-unit length. As seen in (1), the electrical parameters of the line are frequency and space dependent. Assuming that the parameters are constant over a line segment Δx and applying boundary conditions at x and $x+\Delta x$, the following relation between voltages and currents on both sides of the segment is obtained in terms of the chain matrix [20]:

$$\begin{bmatrix}\mathbf{V}(x+\Delta x,s)\\ \mathbf{I}(x+\Delta x,s)\end{bmatrix}=\mathbf{\Phi}(\Delta x,s)\begin{bmatrix}\mathbf{V}(x,s)\\ \mathbf{I}(x,s)\end{bmatrix} \quad (2)$$

The chain matrix of the segment is given by

$$\mathbf{\Phi}(\Delta x,s)=\begin{bmatrix}\cosh(\mathbf{\Psi}\Delta x) & -\mathbf{Y}_0^{-1}\sinh(\mathbf{\Psi}\Delta x)\\ -\mathbf{Y}_0\sinh(\mathbf{\Psi}\Delta x) & \mathbf{Y}_0\cosh(\mathbf{\Psi}\Delta x)\mathbf{Y}_0^{-1}\end{bmatrix} \quad (3)$$

where $\mathbf{\Psi}$ is the propagation constant matrix, computed as

$$\mathbf{\Psi}=\mathbf{M}\sqrt{\boldsymbol{\lambda}}\mathbf{M}^{-1} \quad (4)$$

$\mathbf{M}$ and $\boldsymbol{\lambda}$ are the eigenvalue and eigenvector matrices of the $\mathbf{Z}(x,s)\mathbf{Y}(x,s)$ product, respectively; $\mathbf{Y}_0$ is the characteristic admittance matrix of the line segment computed as

$$\mathbf{Y}_0=\mathbf{Z}(x,s)^{-1}\mathbf{\Psi} \quad (5)$$

The line representing the coil is divided in 5 segments (overhang/2, slot, overhang, slot, overhang/2). The chain matrix from each segment is computed according to (3). It can be noticed that such matrix is a function of the parameters $\mathbf{Z}$ and $\mathbf{Y}$, which are different in the overhang and slot regions.

Finally, the cascaded connection is applied (product of chain matrices) to obtain the chain matrix of the complete coil, as shown in Fig. 2.

The relationship between voltages and currents at the beginning (node S) and end (node R) of the complete coil is obtained as

$$\begin{bmatrix}\mathbf{V}_R\\ \mathbf{I}_R\end{bmatrix}=\mathbf{\Phi}_1\mathbf{\Phi}_2\mathbf{\Phi}_3\mathbf{\Phi}_2\mathbf{\Phi}_1\begin{bmatrix}\mathbf{V}_S\\ \mathbf{I}_S\end{bmatrix}=\begin{bmatrix}\mathbf{\Phi}_{11} & \mathbf{\Phi}_{12}\\ \mathbf{\Phi}_{21} & \mathbf{\Phi}_{22}\end{bmatrix}\begin{bmatrix}\mathbf{V}_S\\ \mathbf{I}_S\end{bmatrix} \quad (6)$$

where $\mathbf{\Phi}_{11}$, $\mathbf{\Phi}_{12}$, $\mathbf{\Phi}_{21}$ and $\mathbf{\Phi}_{22}$ are the elements (submatrices) of the chain matrix of the complete coil. This chain matrix model is transformed into an equivalent nodal form in order to introduce the zig-zag connection required to preserve continuity as the pulse propagates along the turns [20]. This yields:

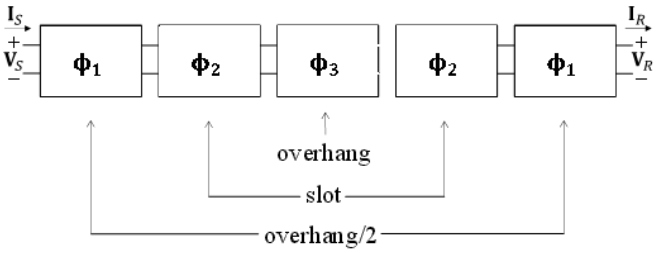

Fig. 2. Cascaded connection of chain matrices to model all regions of coil

$$\begin{bmatrix}\mathbf{V}_S\\ \mathbf{V}_R\end{bmatrix}=\begin{bmatrix}\mathbf{Y}_{SS}+\mathbf{Y}_{con11} & -(\mathbf{Y}_{SR}+\mathbf{Y}_{con12})\\ -(\mathbf{Y}_{SR}+\mathbf{Y}_{con21}) & \mathbf{Y}_{RR}+\mathbf{Y}_{con22}\end{bmatrix}^{-1}\begin{bmatrix}\mathbf{I}_S\\ \mathbf{I}_R\end{bmatrix} \quad (7)$$

where

$$\mathbf{Y}_{SS}=-\mathbf{\Phi}_{12}^{-1}\mathbf{\Phi}_{11} \quad (8)$$

$$\mathbf{Y}_{SR}=-\mathbf{\Phi}_{12}^{-1}=-\mathbf{\Phi}_{22}\mathbf{\Phi}_{12}^{-1}\mathbf{\Phi}_{11}+\mathbf{\Phi}_{21} \quad (9)$$

$$\mathbf{Y}_{RR}=-\mathbf{\Phi}_{22}\mathbf{\Phi}_{12}^{-1} \quad (10)$$

$$\mathbf{Y}_{con11}=\begin{bmatrix}Y_S & 0 & \cdots & \cdots & 0\\ 0 & Y_{con} & 0 & 0 & \vdots\\ \vdots & 0 & \ddots & 0 & \vdots\\ \vdots & \vdots & 0 & \ddots & 0\\ 0 & 0 & 0 & 0 & Y_{con}\end{bmatrix} \quad (11)$$

$$\mathbf{Y}_{con12}=\begin{bmatrix}0 & \cdots & \cdots & \cdots & 0\\ Y_{con} & 0 & \cdots & \cdots & \vdots\\ 0 & \ddots & \ddots & \cdots & \vdots\\ \vdots & 0 & \ddots & \ddots & \vdots\\ 0 & 0 & 0 & Y_{con} & 0\end{bmatrix} \quad (12)$$

$$\mathbf{Y}_{con21}=\begin{bmatrix}0 & Y_{con} & 0 & \cdots & 0\\ \vdots & 0 & \ddots & \ddots & \vdots\\ \vdots & \vdots & 0 & \ddots & 0\\ \vdots & \vdots & \vdots & 0 & Y_{con}\\ 0 & 0 & 0 & 0 & 0\end{bmatrix} \quad (13)$$

$$\mathbf{Y}_{con22}=\begin{bmatrix}Y_{con} & 0 & \cdots & \cdots & 0\\ 0 & \ddots & 0 & \cdots & \vdots\\ \vdots & 0 & \ddots & 0 & \vdots\\ \vdots & \vdots & 0 & Y_{con} & 0\\ 0 & 0 & 0 & 0 & Y_L\end{bmatrix} \quad (14)$$

In (11) - (14), Y_{con} is the (large) admittance introduced for the zigzag connection, Y_S is the source admittance, and Y_L is the admittance corresponding to the rest of the winding ($1/R_{term}$).

The frequency domain nodal voltages obtained from (7) are transformed into the time domain by means of the numerical Laplace transform [23].

III. Modeling of Connection Cable

Accurate modeling of the cable in the inverter-cable-coil setup is very important for a correct prediction of the winding's response. Fig. 3 shows the model used in this work, which corresponds to an equivalent circuit in the frequency domain obtained from short and open circuit measurements using an LCR meter (Agilent E4980) [17]. The parameters of the single-phase cable model are calculated from the short circuit impedance Z_{sc} and open circuit impedance Z_{oc} measured at low and high frequencies (f_{low} and f_{high}, respectively), considering a 1 m long unshielded four-wire cable, size 10 AWG. The cable parameters are obtained as follows [17]:

$$R_s = \frac{2}{3}\text{Real}\{Z_{sc}\}_{flow} \tag{15}$$

$$L_s = \frac{2}{3}\frac{1}{2\pi f_{high}}\text{Imag}\{Z_{sc}\}_{fhigh} \tag{16}$$

$$R_{p1} = 2(\text{Real}\{Z_{oc}\}_{flow})\left[\left(\frac{\text{Imag}\{Z_{oc}\}_{flow}}{\text{Real}\{Z_{oc}\}_{flow}}\right)^2 + 1\right] \tag{17}$$

$$R_{p2} = 2(\text{Real}\{Z_{oc}\}_{fhigh})\left[\left(\frac{\text{Imag}\{Z_{oc}\}_{fhigh}}{\text{Real}\{Z_{oc}\}_{fhigh}}\right)^2 + 1\right] \tag{18}$$

$$C_{p2} = \left[(2\pi f_{high})\left(\frac{\text{Real}\{Z_{oc}\}_{fhigh}}{\text{Imag}\{Z_{oc}\}_{fhigh}}\right)R_{p2}\right]^{-1} \tag{19}$$

$$C_{p1} = \left[(2\pi f_{low})\left(\frac{\text{Real}\{Z_{oc}\}_{flow}}{\text{Imag}\{Z_{oc}\}_{flow}}\right)R_{p2}\right]^{-1} - C_{p2} \tag{20}$$

The series impedance and shunt admittance per unit length of the cable are defined as

$$Z = R_s + sL_s \tag{21}$$

$$Y = \frac{1}{R_{p1}} + \frac{1}{R_{p2} + \frac{1}{sC_{p2}}} + sC_{p2} \tag{22}$$

These parameters are introduced into the distributed parameter admittance model of the cable as follows:

$$\begin{bmatrix} I_S \\ I_R \end{bmatrix} = \begin{bmatrix} Y_{SS} & Y_{SR} \\ Y_{RS} & Y_{RR} \end{bmatrix}\begin{bmatrix} V_S \\ V_R \end{bmatrix} \tag{23}$$

where V_S, I_S and V_R, I_R are the voltages and currents and the sending and receiving ends of the cable, respectively. The elements of the admittance matrix are defined as

$$Y_{SS} = Y_{RR} = Y_0\coth(\gamma L) \tag{24}$$

$$Y_{SR} = Y_{RS} = -Y_0\,\text{csch}(\gamma L) \tag{25}$$

where

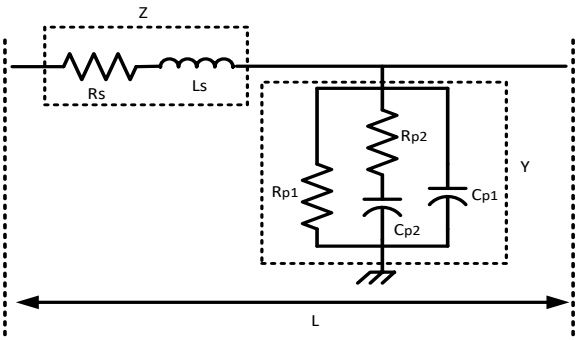

Fig. 3. Equivalent circuit per unit length of the cable

$$\gamma = \sqrt{ZY} \tag{26}$$

$$Y_0 = \sqrt{\frac{Y}{Z}} \tag{27}$$

IV. Case Study

A. Geometrical Configuration

A schematic cross section of the coil considered in this study is shown in Fig. 4. The main parameters of the stator coil are summarized in Table I.

Fig. 5 shows a picture of the experimental setup. Besides the medium-voltage form-wound coil under test, it includes a waveform generator, an oscilloscope, the connection cable and a 100 Ω load connected at the end of the coil. Steel plates were included to emulate the electromagnetic field distribution in the slot region [24]. The experimental setup was placed in a laboratory facility free of electromagnetic interference.

TABLE I
Machine parameters

Turns per stator coil	7
Length of overhang region	0.33 m
Conductor width (w)	5.35 mm
Conductor height (h)	2.85 mm
Resistivity of stator bar conductor	1.7×10-8 Ω·m
Thickness of interturn insulation (δ_1)	0.2 mm
Thickness of main insulation (δ_2)	1.41 mm
Thickness of ground wall insulation (δ_3)	0.36 mm
Relative permittivity of the interturn insulation	2.5
Relative permittivity of the main insulation	2
Relative permittivity of the ground wall ins.	2.8
Slot width (W)	8.9 mm
Slot Height (H)	24.2 mm
Slot length	0.45 m

B. Computation of electrical parameters

A single coil is considered as the basic element for the calculation of machine parameters. As mentioned before, each coil can be divided in two sections: overhang and slot. The capacitance, inductance, and resistance matrices in both coil regions are calculated using the FEM-based software COMSOL Multiphysics.

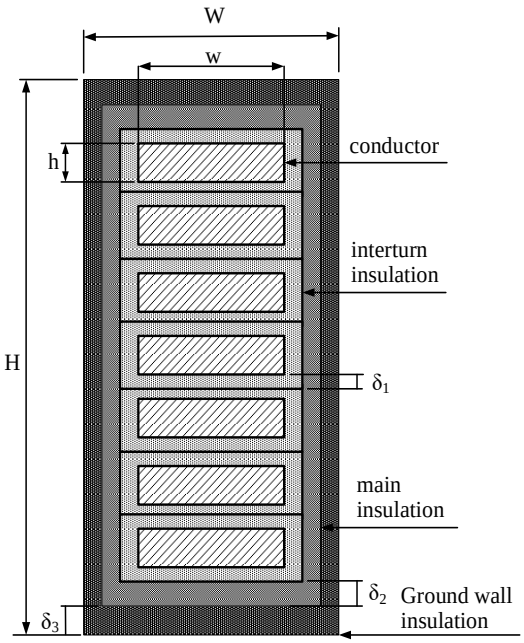

Fig. 4. Cross section of the coil with 3 insulation layers

Fig. 5. Experimental setup for validation of the inverter-cable-coil setup.

In the slot region the slot walls behave as magnetic insulation for the high frequencies related to the fast transient response of the coil. In the overhang region, these walls are replaced by an open boundary condition. The capacitance matrix **C** is calculated using the forced voltage method in the electrostatics module of COMSOL, as shown in Fig. 6 for the first turn. The inductance matrix **L** is calculated using the magnetic energy method, as shown in Fig. 7 also for the first turn. The series losses in the coil (**R**) are computed from the concept of complex penetration depth. The dielectric losses matrix (**G**) is computed using the "electric currents" module in COMSOL.

C. Simulated and experimental results

Initially, the cable and winding models are assessed separately by means of comparisons with experimental measurements.

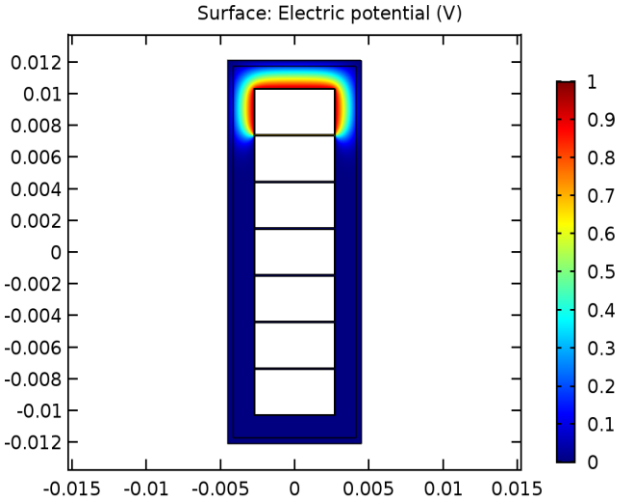

Fig. 6. Capacitance calculation using forced voltage method in FEM

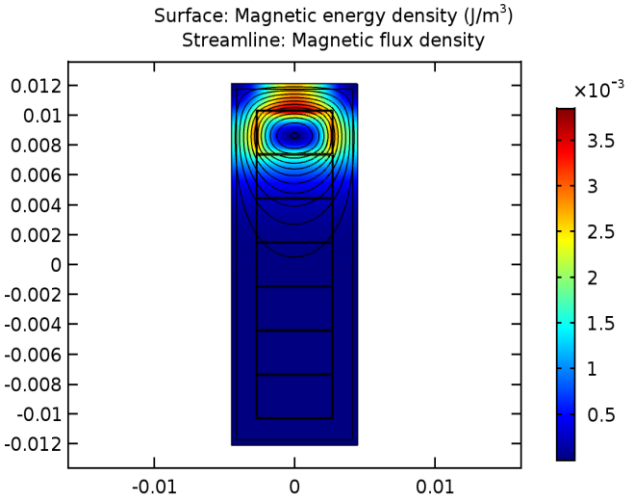

Fig. 7. Inductance calculation using magnetic energy method in FEM

The cable model is validated by means of the simulation of its step response, considering a unit step with rise time of 100 ns at the sending node and a load of 50 Ω connected at the receiving node. The voltage at the receiving end of the cable and its comparison with the experimental measurement are shown in Fig. 8.

The winding model is validated considering a PWM-type excitation with different rise times between 100 and 500 ns connected to the first turn of the coil. The rest of winding is represented by a 100 Ω load. This type of excitation is obtained from the waveform generator emulating the phase to ground voltage from a 5-level voltage source inverter [16]. The corresponding waveform is shown in Fig. 9.

Fig. 10 shows the comparison of the simulated and measured transient voltage at the first winding turn. A second assessment of the winding corresponds to a similar setup, but with an open ended condition of the coil. This results in noticeable oscillations which are reproduced in a very accurate manner by the winding model, as shown in Fig. 11, which illustrates the transient response at the far end of the winding.

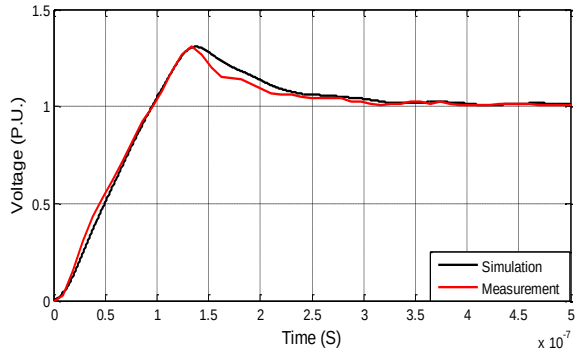

Fig. 8. Transient voltage at the receiving end of the cable

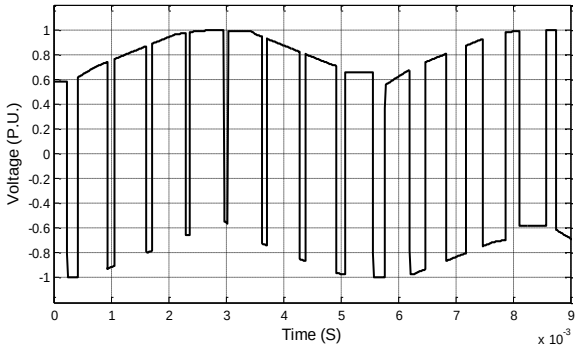

Fig. 9. Typical PWM-waveform generated by an inverter

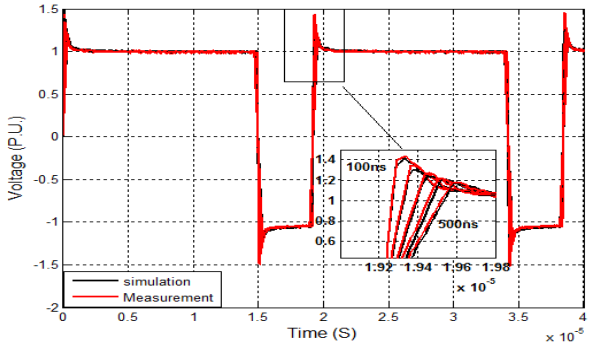

Fig. 10. Transient overvoltage at the first turn of the coil terminated in 100 Ω load

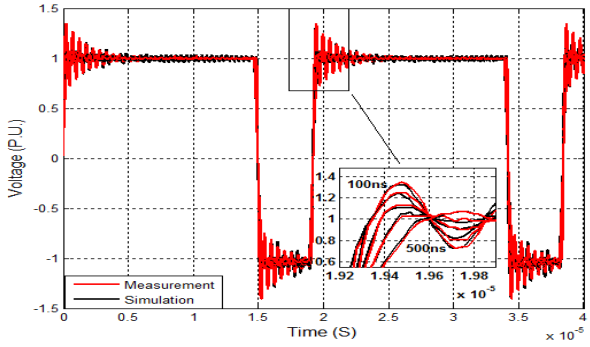

Fig. 11. Transient overvoltage at the last turn of the coil for open ended case.

The following set of simulations correspond to the response of the coil for different rise times of the PWM-type excitation and for different lengths of the connecting cable.

When connecting the inverter to the machine winding coil through a 1-meter cable, the overvoltages are increased, as shown in Fig. 12. This figure corresponds to a PWM-type excitation with 100 ns of rise time, comparing the results with and without cable. In addition, Fig. 13 shows the results for different rises times and 1-meter cable included. These figures also show that, when compared to the experimental results, the simulations corresponding the excitation-cable-machine winding setup produce very accurate results.

The effect of the excitation rise time is analyzed in a more general manner in Fig. 14, which shows the potential difference between turns for different rises times. According to this figure, the potential difference is inversely proportional to the rise time of the excitation.

Finally, the effect of the length of the connection cable is analyzed in Fig. 15, which illustrates the potential difference between turns for an excitation with 100ns of rise time connected to the winding by means of cables of different lengths. According to the results, the potential difference is directly proportional to the cable length.

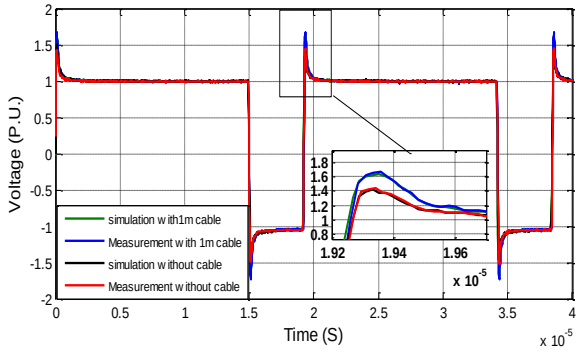

Fig. 12. Transient overvoltage with and without cable.

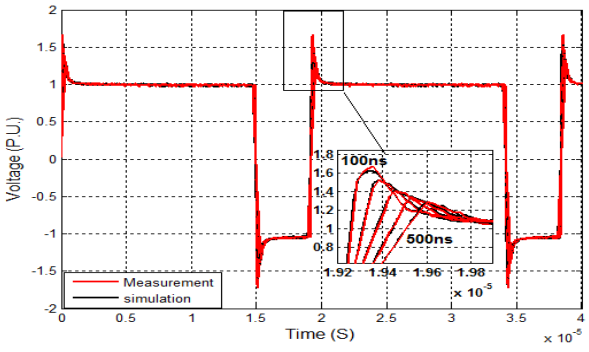

Fig. 13. Transient overvoltage at the first turn of the coil with cable.

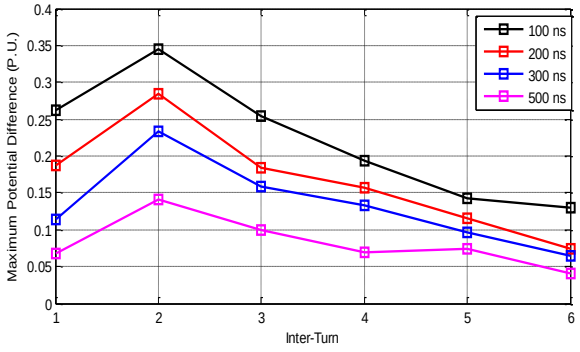

Fig. 14. Potential difference between turns considering different rise times of the excitation.

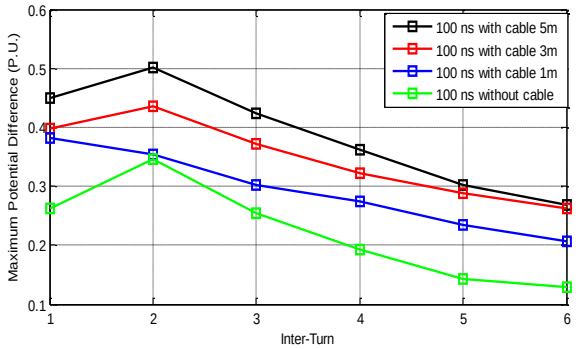

Fig. 15. Potential difference between turns considering different lengths of connection cable.

V. Conclusions

A frequency domain non-uniform multiconductor transmission line approach has been used to study the fast front transient response of a machine winding coil when a PWM-type excitation from an inverter is applied. The parameters of the coil were calculated using the finite element method. The cable connecting the inverter to the winding was included considering a frequency domain distributed parameter model whose parameters are obtained from short and open circuit test measurements.

The results when applying a PWM-type excitation to the coil show that the rise time of the source and length of cable have an important effect on the transient overvoltage produced at different turns of the coil, as well as in the potential difference between adjacent turns. The comparison between simulation and experimental results, in terms of oscillatory behavior and magnitude, demonstrate that both the winding model and the cable model selected result in a very accurate prediction of the fast transient response related to the use of inverters in medium voltage induction machines. Since the winding model is considered as completely linear for high frequencies, a frequency domain modeling approach is a very good option to study the fast transient response of machine windings.

VI. Acknowledgments

The authors would like to thank Dr. Massood Atashbar and Dr. Bradley Bazuin for providing laboratory access to perform experimental validations.

VII. References

[1] V. Venegas, R. Escarela, R. Mota, E. Melgoza, J. L. Guardado, "Calculation of electrical parameters for transient overvoltage studies on electrical machines," in Proc. Electric Machines and Drives Conference, Madison, WI, USA, June 2003, pp. 1978-1982

[2] J. L. Guardado, K. J. Cornick, V. Venegas, J. L. Naredo, E. Melgoza, "A Three-Phase Model For Surge Distribution Studies," IEEE Transactions on Energy Conversion, vol. 12, no. 1, pp. 24-31, 1997.

[3] M. T. Wright, S. J. Yang, K. Yang, "General theory of fast-fronted interturn voltage distribution in electrical machine windings," IEE Proceedings B - Electric Power Applications , vol. 130, no. 4, pp. 245-256, 1983.

[4] P. G. McLaren, H. Oraee, "Multiconductor transmission-line model for the line-end coil of large AC machines," IEE Proceedings B - Electric Power Applications, vol. 132, pp. 149-156, 1985.

[5] J. L. Guardado, K. J. Cornick, "A Computer Model For Calculating Steep-Fronted Surge Distribution In Machine Windings," IEEE Transactions on Energy Conversion, vol. 4, no. 1, pp. 95-101, 1989.

[6] C. Petrarca, G. Lupo, L. Egiziano, V. Tucci, M. Vitelli, "Steep-fronted overvoltages in inverter-fed induction motors: Numerical Identification of Critical Parameters," in Proc. High Voltage Engineering Symposium, London, UK, August 1999, pp. 433-436.

[7] C. Petrarca, G. Lupo, V. Tucci, M. Vitelli, "MTL Model and Fem Package for the Evaluation of Steep-Front Surges Distribution in Machine Windings," in Proc. Conference on Electrical Insulation and Dielectric Phenomena, Ontario, Canada, Oct. 2001, pp. 685-688.

[8] G. Lupo, C. Petrarca, M. Vitelli, V. Tucci, "Multiconductor Transmission Line Analvsis of Steep-front Surges in Machine Windings," IEEE Transactions on Dielectrics and Electrical Insulation, vol. 9, no. 3, p. 467, 2002.

[9] C. Petrarca, A. Maffucci, V. Tucci, M. Vitelli, "Analysis of the voltage distribution in a motor stator winding subjected to steep-fronted surge voltages by means of a multiconductor lossy transmission line model," IEEE Transactions on Energy Conversion , vol. 19, no. 1, pp. 7-17, 2004.

[10] J. L. Guardado, K. J. Cornick, "Calculation Of Machine Winding Electrical Parameters At High Frequencies For Switching Transient Studies," IEEE Transactions on Energy Conversion, vol. 11, no. 1, pp. 33-40, 1996.

[11] T. G. Arora, M. V. Aware , D. R. Tutakne, "Effect of pulse width modulated voltage on induction motor insulation," in Proc. IEEE Conference on Industrial Electronics and Applications (ICIEA), Singapore, 2012, pp. 2044-2048

[12] C. J. Melhorn, L. Tang, "Transient effects of PWM drives on induction motors," IEEE Transactions on Industry Applications, vol. 33, no. 4, pp. 1065-1072, Jul/Aug 1997.

[13] B. S. Basavaraja, B; D. V. Sarma, "Modelling, Simulation and Experimental Analysis of Transient Terminal Overvoltage in PWM-Inverter fed Induction Motors," in Proc. 2007 IEEE Power Engineering Society General Meeting, Tampa, FL, USA, June 2007.

[14] H. De Paula, M. L. R. Chaves, D.A. Andrade, J. L. Domingos , M. A. A. Freitas, "A new strategy for differential overvoltages and common-mode currents determination in PWM induction motor drives," in Proc. IEEE International Conference on Electric Machines and Drives, San Antonio, TX, USA, Dec. 2005, pp. 1075-1081.

[15] A. von Jouanne, P. Enjeti, W. Gray, "The effect of long motor leads on PWM inverter fed AC motor drive systems," in Proc. Applied Power Electronics Conference and Exposition, Dallas, TX, USA, March 1995, pp. 592-597.

[16] F. P. Espino, P. Gomez. D. Betanzos, "Modeling of the Heat Generation on Stress Grading Coatings of Motors Fed by Multilevel Drives", IEEE Transactions on Dielectrics and Electrical Insulation, Vol. 18, No. 4, pp. 1328-1333, August 2011.

[17] A. F. Moreira, T. A. Lipo, G. Venkataramanan, S. Bernet, "High-frequency modeling for cable and induction motor overvoltage studies in long cable drives," IEEE Transactions on Industry Applications,, vol. 38, no. 5, pp. 1297-1306, Sep/Oct 2002.

[18] L. Wang, C. Ngai-Man Ho, F. Canales, J. Jatskevich, "High-Frequency Modeling of the Long-Cable-Fed Induction Motor Drive System Using TLM Approach for Predicting Overvoltage Transients," IEEE Transactions on Power Electronics, vol. 25, no. 10, pp. 2653-2664, Oct. 2010.

[19] P. Gómez, P. Moreno, J. L. Naredo, "Frequency-Domain Transient Analysis of Nonuniform Lines With Incident Field Excitation," IEEE Transactions on Power Delivery, vol. 20, no. 3, p. 2273-2280, July 2005.

[20] M. K. Hussain and P. Gomez, "Modeling of Machine Coils Under Fast Front Excitation Using a Non-Uniform Multiconductor Transmission Line Approach," in Proc. North American Power Symposium (NAPS), Denver, CO, Sept. 2016.

[21] P. Moreno, P. Gomez, M. Davila, J. L. Naredo, "A Uniform Line Model for Non-Uniform Single-Phase Lines with Frequency Dependent Electrical Parameters," in Proc. Transmission & Distribution Conference and Exposition, Caracas, Venezuela, Aug. 2006.

[22] P. Gómez, J. C. Escamilla, "Frequency domain modeling of nonuniform multiconductor lines excited by indirect lightning," International Journal of Electrical Power & Energy Systems, vol. 45, no. 1, pp. 420-426, 2013.

[23] P. Gómez, F. A. Uribe, "The numerical Laplace transform: An accurate technique for analyzing electromagnetic transients on power system devices," International Journal of Electrical Power & Energy Systems, vol. 31, no. 2-3, pp. 116-123, 2009.

[24] S. Ul Haq, M. K. W. Stranges and B. Wood, "A Proposed Method for Establishing Partial Discharge Acceptance Limits on API 541 and 546 Sacrificial Test Coils," IEEE Transactions on Industry Applications, vol. 53, no. 1, pp. 718-722, Jan-Feb 2017.